



## ViVGG19: Novel exemplar deep feature extraction-based shoulder rotator cuff tear and biceps tendinosis detection using magnetic resonance images

Sefa Key<sup>a</sup>, Sukru Demir<sup>b</sup>, Murat Gurger<sup>b</sup>, Erhan Yilmaz<sup>b</sup>, Prabal Datta Barua<sup>c,d</sup>, Sengul Dogan<sup>e,\*</sup>, Turker Tuncer<sup>e</sup>, N. Arunkumar<sup>f</sup>, Ru-San Tan<sup>g,h</sup>, U Rajendra Acharya<sup>i,j,k</sup>

<sup>a</sup> Department of Orthopedics, Bingol State Hospital, Ministry of Health, Bingol, Turkey

<sup>b</sup> Department of Orthopedics, Fırat University Hospital, Fırat University, Elazig, 23119, Turkey

<sup>c</sup> School of Business (Information System), University of Southern Queensland, Toowoomba, QLD 4350, Australia

<sup>d</sup> Faculty of Engineering and Information Technology, University of Technology Sydney, Sydney, NSW 2007, Australia

<sup>e</sup> Department of Digital Forensics Engineering, College of Technology, Fırat University, Elazig, Turkey

<sup>f</sup> Rathinam College of Engineering, Coimbatore, India

<sup>g</sup> Department of Cardiology, National Heart Centre Singapore, Singapore

<sup>h</sup> Duke-NUS Medical School, Singapore

<sup>i</sup> Ngee Ann Polytechnic, Department of Electronics and Computer Engineering, 599489, Singapore

<sup>j</sup> Department of Biomedical Engineering, School of Science and Technology, SUSS University, Singapore

<sup>k</sup> Department of Biomedical Informatics and Medical Engineering, Asia, University, Taichung, Taiwan

### ARTICLE INFO

#### Keywords:

Rotator cuff tear detection  
Biceps tendinosis detection  
Deep feature extraction  
ViVGG19  
Iterative feature selection  
Classification  
Machine learning

### ABSTRACT

**Background and purpose:** : Rotator cuff tear (RCT) and biceps tendinosis (BT) are the two most common shoulder disorders worldwide. These disorders can be diagnosed using magnetic resonance imaging (MRI), but the expert interpretation is manual, time-consuming, and subjected to human errors. Therefore, a fixed-size feature extraction model was created to objectively and accurately perform automated binary classification of RCT vs. normal and BT vs. normal on MRI images.

**Materials and methods:** : We have developed an exemplar deep feature extraction model to diagnose RCT and BT disorders. The model was tested on a new MR image dataset comprising transverse, sagittal, and coronal MRI images of the shoulder that had been organized into three cases. BT was studied on transverse MRI images (Case 1), while RCT was studied on sagittal (Case 2) and coronal MRI images (Case 3). Our model comprised deep feature generation using a pre-trained VGG19, feature selection using iterative neighborhood component analysis (INCA), and classification using shallow standard classifiers k-nearest neighbors (KNN), support vector machine (SVM), and artificial neural network (ANN). In the feature extraction phase, two fully connected layers were used to extract deep features from the original image, and sixteen fixed-size patches obtained by the division of the original image. This model was named Vision VGG19 (ViVGG), analogous to vision transformers (ViT). The feature vector is extracted from the raw image dataset, and 16 feature vectors are extracted from each fixed-size patch. Seventeen feature vectors obtained from each image are obtained from fc6 and fc7 layers of the pre-trained VGG19, are merged to obtain final feature vector. INCA was used to choose the top features from the created features, and the chosen features were classified using shallow classifiers.

**Results:** : We defined three cases to evaluate the proposed ViVGG19 to diagnose RT and BCT disorders. Our proposed ViVGG19 model achieved more than 99% accuracy using the KNN classifier.

**Conclusions:** : ViVGG19 is a very effective model for detecting RCT and BT disorders on shoulder MRI images. The developed automated system is ready to be tested with a bigger diverse database obtained from different medical centers.

\* Corresponding author.

E-mail address: [sdogan@firat.edu.tr](mailto:sdogan@firat.edu.tr) (S. Dogan).

## 1. Introduction

A common cause of anterior shoulder pain is pathology affecting the long head of the biceps tendon (LHBT) [1]. Surgical treatment may be required for symptomatic patients who do not respond to conservative treatment. In selecting patients for surgical treatment, the severity and duration of symptoms as well as individual patient characteristics constitute key considerations [2]. Biceps tenotomy or tenodesis is the standard surgical procedure for treating biceps tendinosis (BT). Speed and Yergason's tests may be used to diagnose LHBT disease on physical examination but possess only modest diagnostic sensitivity (32% and 43%, respectively) [3]. Pinpointing the exact cause of shoulder pain can be difficult. As LHBT pathology may co-exist with other shoulder pathologies, LHBT disease may be overlooked because of another major pathology, and the physical examination findings can be nonspecific or confusing. Diagnostic arthroscopy is the most accurate, but it is generally avoided at the initial workup due to its invasive nature. Various noninvasive imaging modalities, such as ultrasonography and magnetic

resonance imaging (MRI), are frequently used in orthopedics to identify the underlying pathology of shoulder pain and select appropriate treatment. Real-time dynamic ultrasonography can detect LHBT pathology sensitively, but its diagnostic utility drops significantly for partial tears [4]. MRI offers good spatial resolution and exquisite soft-tissue characterization and is thus more accurate for diagnosing LHBT disease [5].

The rotator cuff, consisting of the supraspinatus, infraspinatus, subscapularis, and teres minor tendons, plays a vital role in controlling shoulder movements and stabilizing the shoulder joint. Rotator cuff tear (RCT) causes severe shoulder pain and limitation of movement. Its incidence is expected to increase with improving life expectancy [6]. It is challenging to locate the site of RCT tear precisely on physical examination alone, which underscores the importance of confirmatory imaging diagnosis. Today, MRI is recommended as first-choice imaging for both suspected rotator cuff and biceps tendon injuries, as well as in most intra-shoulder pathologies [7] [8]. Arthroscopy is considered the gold standard for diagnosing RCT, but it is invasive, expensive, and,

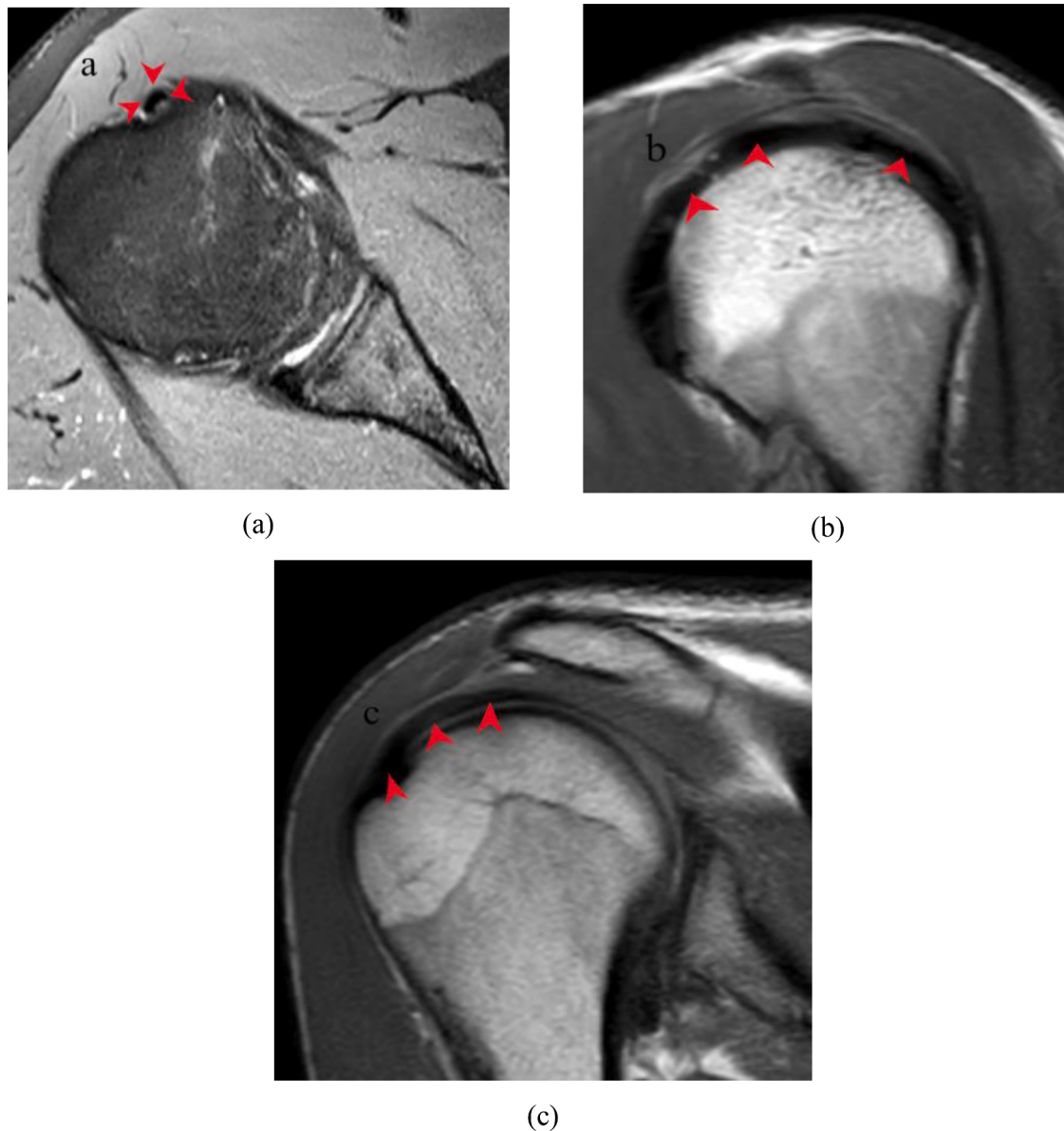


**Fig. 1.** Normal MRI appearance of the biceps tendon and rotator cuff. (A) Tendon in the bicipital groove on T2-weighted axial MRI shows high signal intensity (arrowheads). (B) Normal rotator cuff appearance on parasagittal MR images (arrowheads). (C) Normal rotator cuff appearance on coronal oblique MRI images (arrowheads).

S. Key et al.

Medical Engineering and Physics 110 (2022) 103864

therefore, not suitable for routine use.

MRI offers high resolution, excellent soft-tissue characterization, high sensitivity and high specificity [8]. Typical MRI images of normal and after shoulder injury areas are shown in Fig. 1 and Fig. 2, respectively.

In rotator cuff tears, fat-suppressed MRI T2-weighted images may detect an increase in signal between tendon fibers, decrease in tendon diameter for partial tears, and deterioration in tendon continuity in full-thickness tears. Full-thickness tears lead to communication between the glenohumeral joint and the subacromial space. Fat-suppressed T2-weighted image shows the lesions more clearly as the tendon tear becomes filled with fluid. Large rotator cuff tears usually involve the supraspinatus muscle, infraspinatus muscle, or subscapular muscle, and retraction may be observed [9]. When evaluating intra-shoulder pathologies of the biceps tendon, a T2-weighted parasagittal MRI image is examined. On MRI, the tendon shows mild contour irregularity and heterogeneous high signal intensity in two consecutive images, that is, in two consecutive sections. T2-weighted axial MRI shows high signal

intensity surrounding the tendon and effusion in the bicipital groove [10] (Fig. 2).

MRI is typically manually interpreted by radiologists and orthopedic specialists. The interpretation of image features is dependent on the reader's experience. There is intra- and interobserver variability, and the margin of error may affect the accuracy of diagnosis. Computer-aided diagnostic systems can be used as an objective method to screen for pathologies on MRI, which may reduce the time cost of experts and improve accuracy.

### 1.1. Motivation and our model

Biomedical computer vision has found important applications in medical image diagnosis in diverse imaging modalities like MRI, computed tomography (CT), and X-ray. In this work, we focused on the automated detection of two orthopedic conditions, RCT and BT. A new dataset was created using axial, sagittal, and coronal sections, which were organized into three evaluation cases (see Table 1). Shoulder

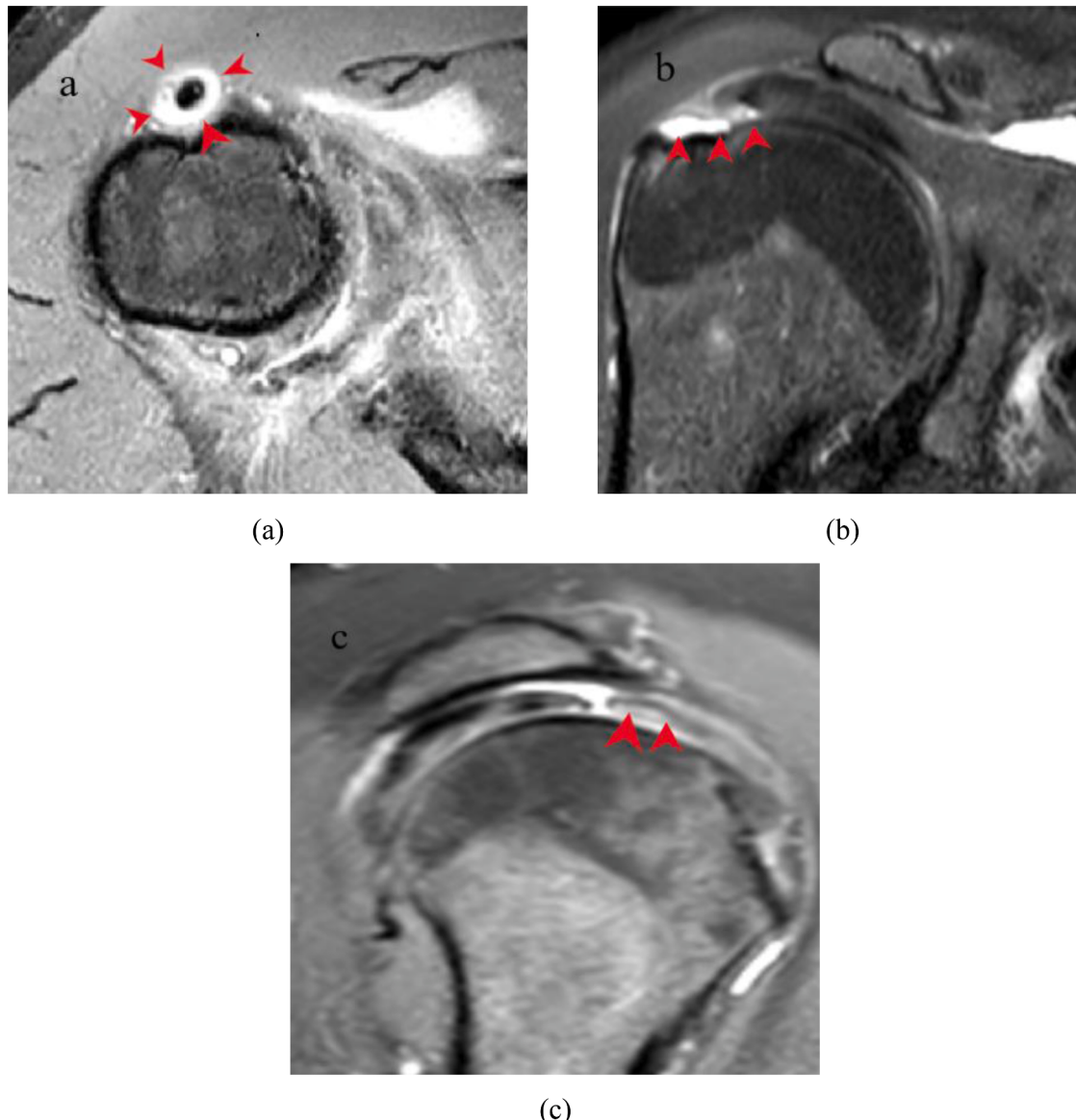


**Fig. 2.** MRI appearance of rotator cuff tear and biceps tendinosis. (A) T2-weighted axial MRI with high signal intensity surrounding the tendon and effusion in the bicipital groove (arrowheads). (B) The increased signal between tendon fibers and decreased tendon diameter for rotator cuff tear on coronal oblique fat-suppressed T2-weighted MRI images (arrowheads). (C) The increased signal between tendon fibers and decreased tendon diameter for rotator cuff tears on T2-weighted parasagittal MRI images (arrowheads).

**Table 1**

Details of the dataset used for this work.

Image orientation/ Disorder	Number of images with the disorder	Number of images with no disorder	Total number of images
Transverse/ BT (Case 1)	155	140	295
Sagittal/ RCT (Case 2)	234	172	406
Coronal/ RCT (Case 3)	263	205	468

\*Differences in the total number of images are due to the removal of images with poor quality in sections in MRI.

ailments have generally been seen as orthopedic disorders, and these ailments should be diagnosed rapidly to give the most suitable treatment. Moreover, there are limited machine learning-based applications in orthopedics. We have proposed an automated RCT and BT detection model to get quick diagnosis results.

To get results from the created three cases, we were inspired by the approach used in vision transformers (ViT) [11–14]. In the ViT, fixed-size patch-based classification was employed. We divided the images into patches in this study and used pre-trained VGG19 [15] to generate deep features. VGG19 [15] is one of the most used deep learning models in the literature and has yielded variable high classification performances for various computer vision problems. Therefore, we selected this CNN to extract deep features. In ViT, an attention transformer has been used to extract features. In this work, we used pre-trained VGG19 to extract features and investigated the performance of the VGG19 in this architecture.

An iterative feature selector, iterative neighborhood component analysis (INCA) [16], was used to select the top features, which were then fed to three shallow classifiers, KNN [17], support vector machine (SVM) [18, 19], and artificial neural network (ANN) [20].

Moreover, a schematic model overview of this model is given in Fig. 3.

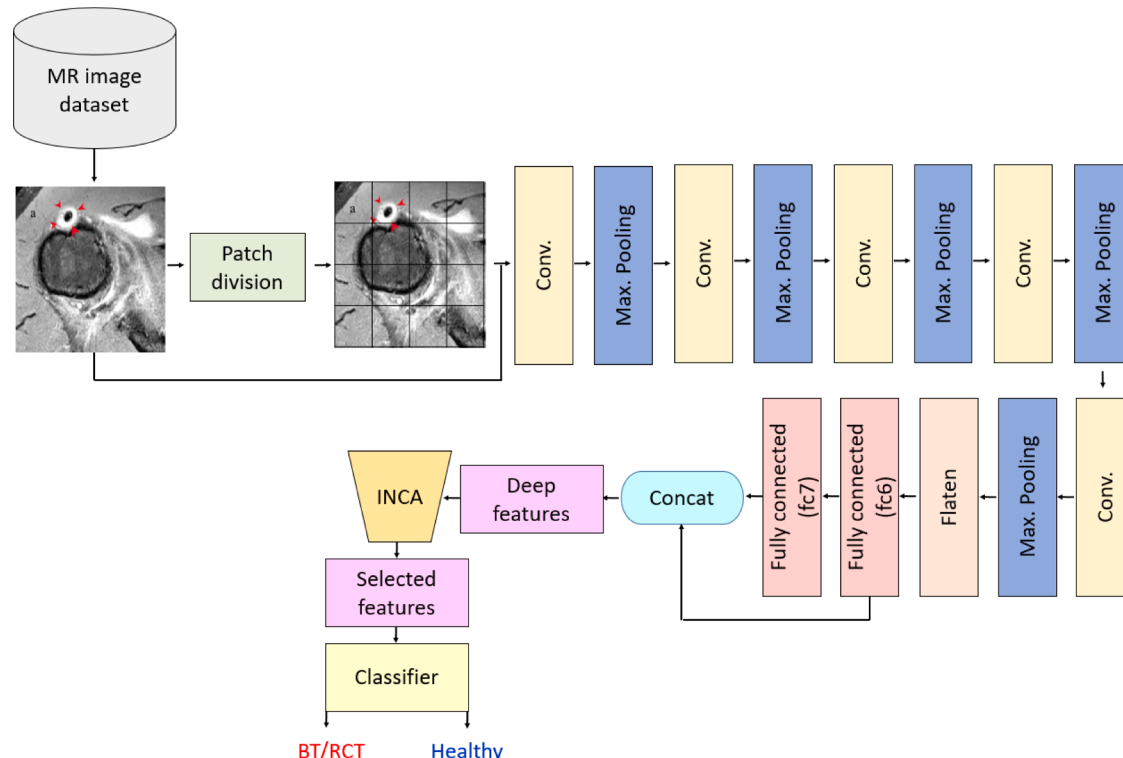


Fig. 3. An overview of the ViVGG19 model.

## 2. Dataset and collection method

The dataset comprised MRI images of 112 unique patients (there are 66 females and 46 males) aged 18 years and above (maximum age is 72 and general age is calculated as  $46.17 \pm 15.96$ ) with BT or RCT who attended the Firat University Hospital Orthopedics and Traumatology Clinic between January 2015 and January 2020. We retrospectively identified BT and RCT patients from orthopedic surgery records and excluded those with previous shoulder surgery, proximal humeral fracture, concomitant inflammatory arthritis, and biceps subluxation or dislocation. The images were acquired on a 3 Tesla MRI scanner (Achieva, Philips Medical Systems). For RCT, three contiguous MRI image slices at both coronal and sagittal views were evaluated; for BT, three contiguous MRI image slices in the transverse plane were used. Three orthopedic surgeons and a senior radiologist reviewed all MRI images. These four professionals labeled all MRIs. Moreover, the accuracy of the MRI findings was compared against the arthroscopy reference standard.

The dataset was organized into three cases with orthogonal image slice orientations, one for BT and 2 for RCT, with a mix of images showing the disorder and no disorder (Table 1). We have used transverse, sagittal, and coronal image orientations. Moreover, we stored each image in jpg format.

## 3. Our proposed ViVGG19

We were inspired by fixed-size-based effective models like ViT [11] and MLP-Mixer [21] to propose a new fixed-size-based deep feature engineering model using a pre-trained VGG19 feature extraction function in the transfer learning mode. This was combined with an iterative feature selection function INCA and three shallow classifiers, KNN, SVM, and ANN. A graphical depiction of the model is shown in Fig. 4.

We resized images to  $224 \times 224$  sizes.  $56 \times 56$  sized patches were used in the fixed-size patch division, which created 16 fixed-size patches for every main resized image. We used the fc6 and fc7 layers in the pre-trained VGG19 to create 8192 features from the main image as well as every patch, i.e., 17 feature vectors (one feature vector has been extracted from raw image and 16 feature vectors have been extracted from created fixed-size patches) each with a length of 8192 features. These features are merged to form a concatenated feature vector with a length of 139,264. INCA was used to choose the most informative features from the 139,264 features generated per original raw image. The chosen features were classified using KNN, SVM, and ANN with 10-fold cross-validation.

The pseudocode of the proposed ViVGG19 has been given in Algorithm 1.

The detailed steps used in the development of the ViVGG19 are given below.

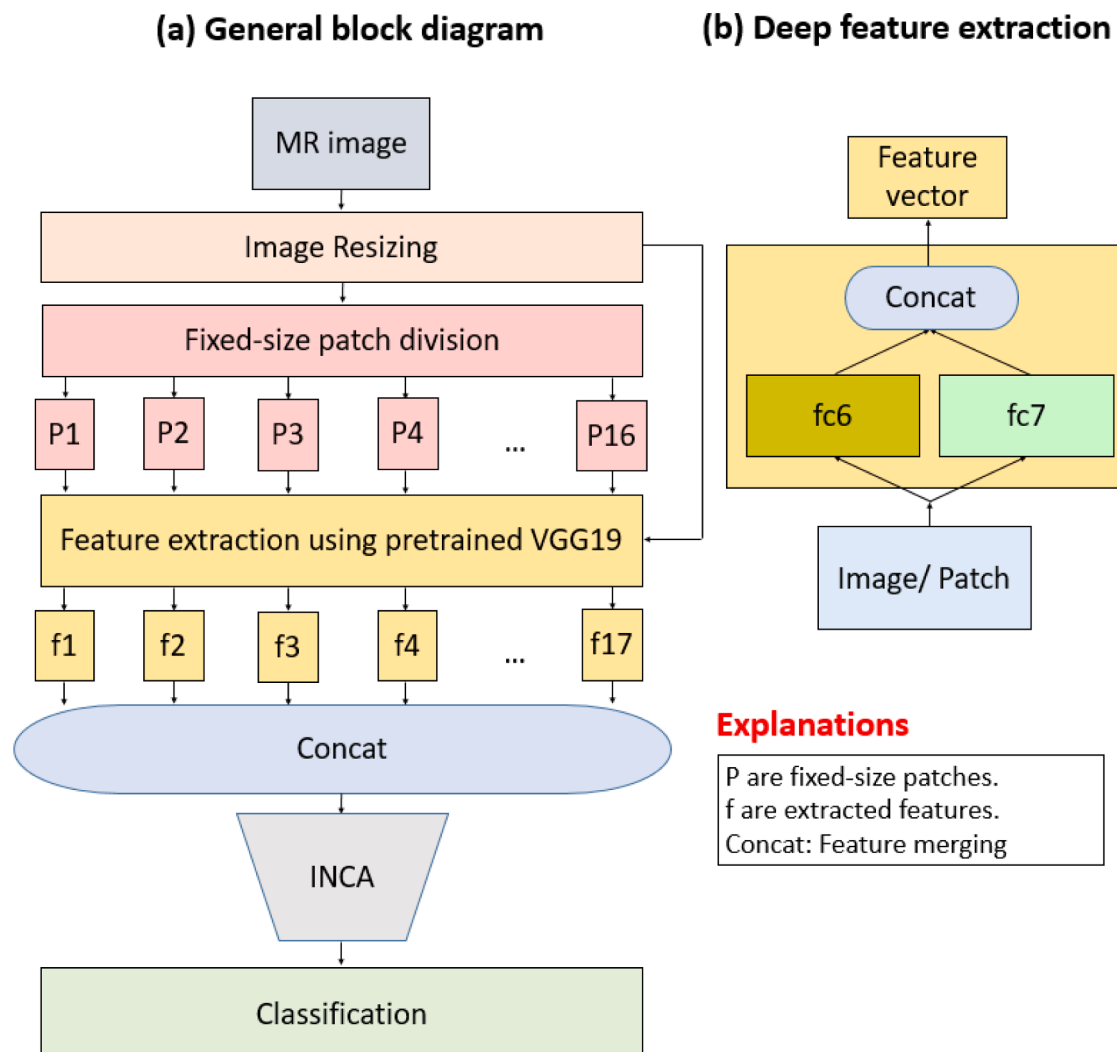


Fig. 4. Graphical outline of the ViVGG19 model.

S. Key et al.

Medical Engineering and Physics 110 (2022) 103864

### 3.1. Feature extraction

**Step 1:** Apply image resizing to the MR image. This step resizes MR images to  $224 \times 224$  sized images.

**Step 2:** Divide the image into  $16 \times 56 \times 56$  sized fixed-size patches. We can also use patches of smaller size, but a huge feature vector will be created due to the larger number of patches.

$$p_c = I(i+k-1, j+k-1), i \in \{1, 2, \dots, 224-55\}, j \in \{1, 2, \dots, 224-55\}$$

$$k \in \{1, 2, \dots, 55\}, c \in \{1, 2, \dots, 16\} \quad (1)$$

Herein,  $p_c$  is  $c^{\text{th}}$  fixed sized patch with a size of  $56 \times 56$ .

**Step 3:** Generate features from the raw MR image by deploying fc6 and fc7 layers of the pre-trained VGG19.

**Step 4:** Generated deep features from each of the created patches.

$$f_1 = concat(fc6(I), fc7(I)) \quad (2)$$

$$f_{c+1} = concat(fc6(p_c), fc7(p_c)), c \in \{1, 2, \dots, 16\} \quad (3)$$

where  $f_c$  represents  $c^{\text{th}}$  feature vector by extracting fc6 and fc7 layers of the pretrained VGG19.  $concat(\cdot)$  is merging function. The length of extracted feature vector ( $f_c$ ) is equal to 8192 ( $=4096+4096$ ).

**Step 5:** Merge the feature vectors created.

$$X = concat(f_1, f_2, \dots, f_{17}) \quad (4)$$

Herein, the extracted all feature vector are merged and concatenated feature vector ( $X$ ) with a length of 139,264 ( $=8192 \times 17$ ).

### 3.2. Feature selection

**Step 6:** Apply the INCA selector to the created features. This feature selection function is an iterative selector. Firstly, NCA calculates the weights of the generated features. A range has been assigned to decrease the time complexity of this selector. Using this range, k feature vectors have been chosen by deploying qualified indices generated by NCA. Loss values of these k feature vectors have been calculated using a classifier. Finally, the best feature vector was chosen using the greedy search method (minimum loss).

### 3.3. Classification

**Step 7:** Classify the chosen features by deploying KNN [17], SVM [18, 19], or ANN [20] with a 10-fold cross-validation strategy.

## 4. Performance evaluation

This section evaluates the performance of the proposed model for the collected datasets.

### 4.1. Experimental setup

The three cases derived from the original dataset (see Table 1) were analyzed separately. The model was implemented in MATLAB 2021b programming environment. Table 2 depicts the parameter settings of the ViVGG19 model.

### 4.2. Cases

We defined three cases (see Table 1) to evaluate our proposed ViVGG19. These cases are defined below.

**Case 1:** To automatically detect BT using transverse MR images. There were 295 axial MR images. In this case, 155 were BT, and 140 were non-BT.

**Table 2**  
Parameters of the ViVGG19.

Phase	Function/method	Parameter(s)
Deep feature creation	Image resizing Fixed-size patch division Feature extraction	$224 \times 224$ $56 \times 56$ Network: VGG19 Layers: fc6, fc7 Mode: Deep features are extracted from patches and MR images.
INCA	Feature merging Range Loss generator Number of features of the chosen optimal feature vectors	Concatenation function [100,500] KNN with a 10-fold CV Case 1: 103 Case 2: 212 Case 3: 316
Classification	KNN	K: 1 Distance: Euclidean Weight: None Validation: 10-fold CV
SVM		Kernel: Cubic Scale: Automatic Coding: One-vs-One Validation: 10-fold CV
ANN		Layer size: 100 Activation function: ReLu Lambda: 0 Validation: 10-fold CV

**Case 2:** To automatically detect RCT using sagittal MR images. There were 406 sagittal MR images, 234 were RCT, and 172 were non-RCT.

**Case 3:** To automatically detect RCT using coronal MR images. There were 468 coronal MR images, 263 were RCT, and 205 were non-RCT.

Each of the three cases posed binary classification problems (disorder seen on image vs. disorder not seen on image).

### 4.3. Validation

In this research, 10-fold cross-validation has been used since this validation technique is one of the most commonly used validator. Moreover, robust results have been calculated by deploying a 10-fold CV.

### 4.4. Performance evaluation metrics

Standard performance metrics accuracy ( $acc$ ), sensitivity ( $sen$ ), specificity ( $spe$ ), geometric mean ( $gm$ ), precision ( $pre$ ), F1-score ( $f1$ ), and balanced accuracy ( $balacc$ ) were used for evaluation of each of the three cases. They can be expressed in terms of the number of true positives ( $tp$ ), false negatives ( $fn$ ), true negatives ( $tn$ ), and false positives ( $fp$ ) as given below [22, 23].

$$acc = \frac{tn + tp}{tn + fn + fp + tp} \quad (5)$$

$$f1 = \frac{2tp}{2tp + fp + fn} \quad (6)$$

$$sen = \frac{tp}{fn + tp} \quad (7)$$

$$pre = \frac{tp}{fp + tp} \quad (8)$$

$$spe = \frac{tn}{fp + tn} \quad (9)$$

$$gm = \sqrt{sen \times spe} \quad (10)$$

S. Key et al.

Medical Engineering and Physics 110 (2022) 103864

$$balacc = \frac{sen + spe}{2} \quad (11)$$

#### 4.5. Results

Three shallow classifiers, KNN, SVM, and ANN, were used. The obtained results of the performance metrics are summarized in Table 3. The best performing classifier was KNN, which achieved 100% classification accuracy rates in Case 1 (BT detection) and Case 3 (RCT detection using coronal images).

#### 4.6. Time complexity

A big O notation has been used to calculate the proposed model's time burden. Time complexity calculation of our proposed is given below.

**Feature extraction:** In this phase, we used an exemplar deep feature generation function and pre-trained VGG19. In this phase, the deep features are extracted from patches. Therefore, the time complexity of the deep feature extraction phase is equal to  $O(nv)$ . Herein,  $n$  is the number of patches, and  $v$  defines the time complexity of the pre-trained VGG19.

**Feature selection:** We used the INCA feature selector. This selector uses three components: range of the loop, loss function, and NCA. Firstly, sorted indices of the features have been calculated by deploying the NCA function. Using these indices, feature vectors have been chosen iteratively. Finally, a loss function has been applied to each feature vector selected, and the best feature vector has been selected by deploying loss values. Thus, the time burden of the INCA is equal to  $O(s + rl)$ . Herein,  $s$  is the time complexity coefficient of the NCA,  $r$  defines the number of the loop, and  $l$  represents the time burden coefficient of the loss function.

**Classification:** We have used a shallow classifier to demonstrate the classification ability of the generated features. These classifiers are ANN, KNN, and SVM and have different time burdens. Thus, we used  $c$  coefficient to define the time complexity of them and the time complexity of the classification phase is equal to  $O(c)$ .

Total: Total time burden of the proposed ViVGG19 image classification model is equal to  $O(nv + s + rl + c)$ . This result demonstrates that our model has linear complexity.

#### 5. Discussion

The rotator cuff and biceps tendon are related anatomical structures provide stability to the shoulder. Therefore, making the correct clinical and arthroscopic diagnoses of BT and RCT is important for determining appropriate treatment. MRI is the noninvasive reference standard for evaluating shoulder diseases. Due to its excellent soft-tissue characterization and multi-plane imaging capability, MRI is increasingly used in the preoperative evaluation of rotator cuff diseases and can identify findings that may have important prognostic implications [24]. However, MRI interpretation can be subjective with wide intra-observer and inter-observer variabilities. In the literature, the overall diagnostic

accuracy rate with expert interpretation of MRI is 89% [25], which is better than that for ultrasound (78% for RCT). In our study, we have developed a model that could accurately classify BT vs. normal as well as RCT vs. normal on MRI scans when referenced against the gold standard of arthroscopic findings. Objective and accurate identification of these pathologies will avert unnecessary diagnostic workup and treatment.

In this work, a new feature extraction model was presented. The model generated deep exemplar features by deploying the pre-trained VGG19. Hence, the presented feature extraction model is named ViVGG19. fc6 and fc7 layers of the pre-trained VGG19 (it was trained on the ImageNet [26] 1 M cluster) were used to generate features from the original image. ViVGG19 was also applied to the divided fixed-size patches derived from the original image to exhaustively extract features. Finally, INCA was used to select the most informative features from the generated feature vector of 139,264 lengths. The feature selection process of the INCA for the defined three cases is illustrated in Fig. 5.

It can be noted from Fig. 5 that Case 1 and Case 3 attained zero error values using 103 and 316 features, respectively. On the other hand, the optimal number of features, error rate, and classification accuracy was 212, 0.049, and 99.51%, respectively, for Case 2.

We have developed our automated system using KNN, SVM, and ANN classifiers with a ten-fold cross-validation strategy. The best and lowest performance for the three cases was obtained using KNN, and ANN classifiers, respectively. All the classifiers yielded excellent results with more than 96% classification accuracy (Table 3).

In addition, we compared our method with other techniques developed for automated shoulder disorder detection using MRI in Table 4.

As can be seen from Table 4, there are limited work done on automated orthopedic disorder diagnosis using machine learning techniques. We have presented an exemplar deep feature extractor to gain high classification ability from the orthopedic images. Using this deep feature extractor, a comprehensive feature vector has been created. INCA eliminates the redundant features. The chosen optimal feature vector coupled with shallow classifiers (KNN, ANN, and SVM) yielded high classification performance. The RCT and BT symptoms are seen in the small area of the images. Our developed methodology could pick up these subtle variations in the small area and attain high classification ability.

The main benefits of our proposed method are as follows:

- From the original dataset, we generated three cases that could be used to study BT and RCT independently.
- A novel deep feature extraction model based on VGG19 was developed and tested.
- Three shallow classifiers were deployed to test the model performance using a ten-fold cross-validation strategy.
- The presented model attained excellent performance, with over 96% classification accuracies for all cases using ANN, KNN, and SVM classifiers.

The limitation of our study is that the dataset used for this was acquired from a single medical center using a small database. In the future,

**Table 3**

Results (%) obtained using our presented ViVGG19 model for three cases with three classifiers by employing 10-fold cross-validation strategy.

Case	Classifier	Acc.	F1	Sen.	Pre.	Spe.	gm	Balacc
Case 1	KNN	100	100	100	100	100	100	100
	SVM	99.66	99.68	100	99.36	99.29	99.64	99.64
	ANN	99.32	99.35	99.35	99.35	99.29	99.32	99.32
Case 2	KNN	99.51	99.57	99.57	99.57	99.42	99.50	99.50
	SVM	97.78	98.08	98.29	97.87	97.09	97.69	97.69
	ANN	96.80	97.20	96.58	97.84	97.09	96.84	96.84
Case 3	KNN	100	100	100	100	100	100	100
	SVM	99.36	99.43	99.62	99.24	99.02	99.32	99.32
	ANN	98.72	98.86	99.24	98.49	98.05	98.64	98.64

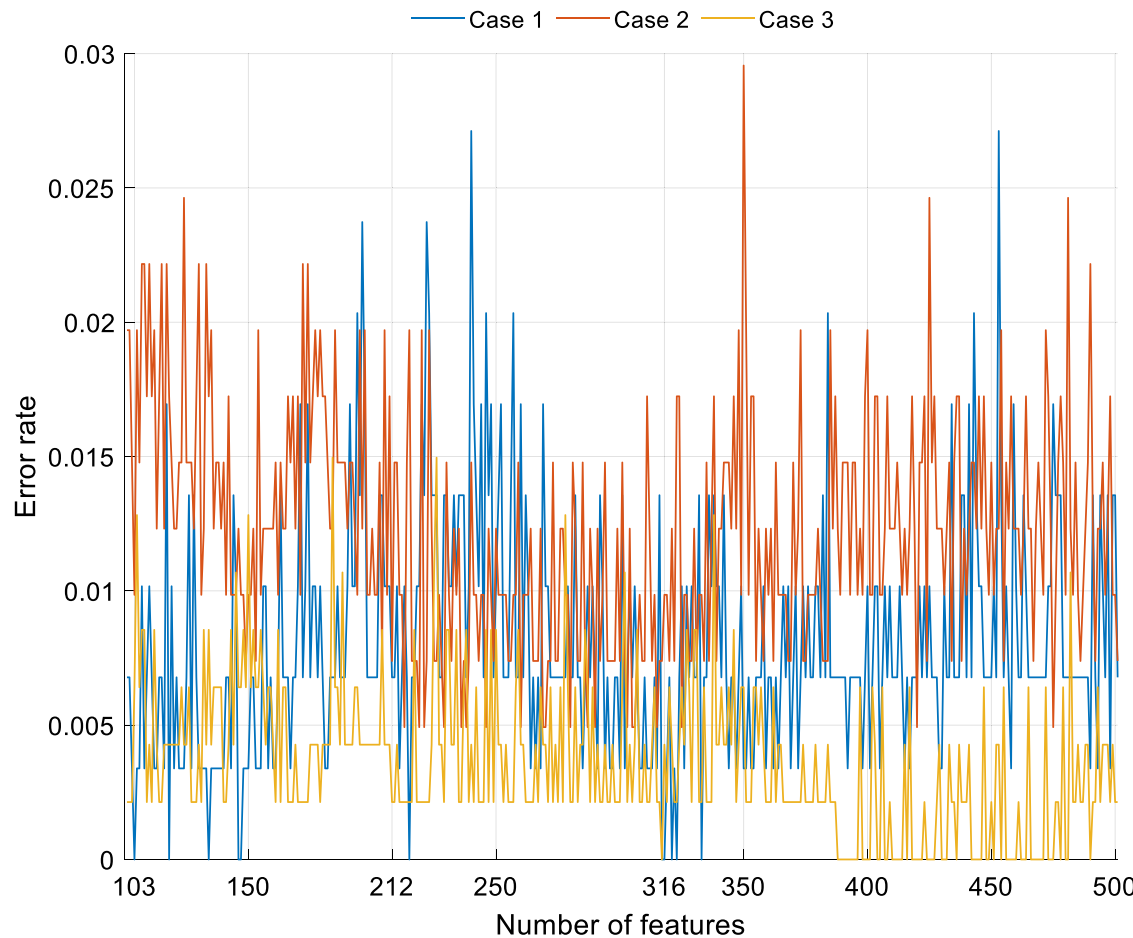


**Fig. 5.** Plot of error rates versus the number of features required for three cases. This figure shows calculated error rates during iterative feature selection. Least loss values are obtained for feature 401 .

**Table 4**  
Comparison of our results with state-of-the-art techniques methods developed.

Study	Method	Purpose	Subjects	Split ratio	Number of classes	The results (%)
Matcuk JR et al. [27]	Statistical analysis ( <i>t</i> -test, <i>p</i> -values), CART	Analysis of patients with and without rotator cuff tears	120 patients with rotator cuff tears 80 normal	80:20	2	Accuracy: 99.50
Jiang et al. [28]	Statistical analysis	Predicting of subacromial impingement syndrome stages	223 early-stage subacromial impingement syndrome 101 advanced stage subacromial impingement syndrome	70:30	2	AUC: 83.90 Sensitivity: 80.30 Specificity: 84.50
Kang et al. [29]	Convolutional neural network	Inflammation severity grading	1024 patients	90:10	2	AUC: 83.00 Sensitivity: 91.40
Our model	Exemplar VGG19 feature extraction	BT and RCT detection	112 patients	10-fold CV	2	Case 1: Accuracy: 100, Case 2: Accuracy: 99.51 Case 3: Accuracy: 100

we intend to collaborate with more medical centers and collect a huge database to develop the model.

## 6. Conclusions

This work introduced a novel deep feature engineering model for

detecting RCT and BT. Three cases were generated from the original dataset, and the MRI images were used to study BT and RCT conditions independently. A deep feature extractor was created by deploying the fc6 and fc7 layers of the pre-trained VGG19. Deep features were extracted from both the original image and subdivided patches of the original image. INCA was employed to select the optimal feature vectors.

S. Key et al.

**Algorithm 1**

Pseudocode of our proposed ViVGG19.

```

Input: Image dataset (db).
Output: Classification results.
01: for k = 1 to N do // Herein, N is the number of the image in the db
02:   I = dbk; // Read each MR image.
03:   Resize I to 224 × 224.
04:   f1 = VGG19(I); // Extract features from the image by deploying VGG19(.)
05:   c = 2; // Define counter
06:   for i = 1 to 224 step by 56, do
07:     for j = 1 to 224 step by 56 do
08:       patch = I(i + 55, j + 55); // Applying patch division.
09:       fc = VGG19(patch); // Extract features from patch by deploying VGG19(.)
10:      c = c + 1;
11:    end for j
12:  end for i
13:  X(k, :) = concat(f1, f2, ..., fc);
// Create final vector (X) and concat() is a concatenation function
14: end for k
15: Apply INCA to X and obtain selected features.
16: Classify selected features by deploying ANN, KKNN, or SVM and obtain classification results.

```

Three classifiers: KNN, SVM, and ANN, were used to evaluate the model performance. KNN classifier attained 100%, 99.51%, and 100% for BT detection, RCT detection using sagittal MRI images, and RCT detection using coronal MRI images, respectively. These results compared favorably with the reported accuracy of medical expert interpretation of about 89% in the literature.

**7. Future works**

Our plan is to collect a large MRI image dataset to apply the model to other orthopedic disorders. Also, a new-generation deep learning model can be trained on the collected huge dataset. A new transfer learning-based intelligent orthopedic disorder detection application can be developed by obtaining the optimal weights. These applications can find potential use in medical centers. The best-suited scenario is given as follows. We will develop a new automated BT and RCT detection application using our proposal, and this application is embedded in MR devices. Most patients have applied to emergency services. These disorders will be diagnosed automatically in emergency services, and the orthopedists' workload will decrease marginally. Thus, orthopedists will be able to devote more time to treatment.

**Funding**

The authors state that this work has not received any funding.

**Institutional review board statement**

This research has been approved on ethical grounds by the Non-Interventional Research Ethics Board Decisions, Firat University on 13 January 2022 (2022-01/08.124143).

**Data availability statement**

The data presented in this study are available on request from the corresponding author. The data are not publicly available due to restrictions regarding the Ethical Committee Institution.

**Ethical approval**

This research has been approved on ethical grounds by the Non-Interventional Research Ethics Board Decisions, Firat University on 13 January 2022 (2022/01-08).

**Declaration of Competing Interest**

The authors of this manuscript declare no conflicts of interest.

**References**

- [1] Elser F, Braun S, Dewing CB, Giphart JE, Millett PJ. Anatomy, function, injuries, and treatment of the long head of the biceps brachii tendon. *Arthroscopy: J Arthroscopic Related Surg* 2011;27:581–92.
- [2] Barber FA, Field LD, Ryu RK. Biceps tendon and superior labrum injuries: decision-making. *JBJS* 2007;89:1844–55.
- [3] Holtby R, Razmjou H. Accuracy of the Speed's and Yergason's tests in detecting biceps pathology and SLAP lesions: comparison with arthroscopic findings. *Arthroscopy: J Arthroscopic Related Surg* 2004;20:231–6.
- [4] Skandzel JG, Jacobson JA, Carpenter JE, Miller BS. Long head of biceps brachii tendon evaluation: accuracy of preoperative ultrasound. *Am J Roentgenol* 2011;197:942–8.
- [5] Dubrow SA, Streit JJ, Shishani Y, Robbin MR, Gobezie R. Diagnostic accuracy in detecting tears in the proximal biceps tendon using standard nonenhancing shoulder MRI. *Open Access J Sports Med* 2014;5:81.
- [6] Via AG, De Cupis M, Spoliti M, Oliva F. Clinical and biological aspects of rotator cuff tears. *Muscles Ligaments Tendons J* 2013;3:70.
- [7] Li W-F, Shakir TM, Zhao Y, Chen T, Niu C, Wang Z. An evidence-based approach to assess the accuracy of MRI in diagnosing rotator cuff Tears: a systematic review and meta-analysis. *Iranian J Radiol* 2019;16.
- [8] Liu F, Cheng X, Dong J, Zhou D, Han S, Yang Y. Comparison of MRI and MRA for the diagnosis of rotator cuff tears: a meta-analysis. *Medicine (Baltimore)* 2020;99.
- [9] Buerba RA, Arshi A, Lee KM, Levine BD, Petrigliano FA. MRI-Arthroscopy correlation of the rotator cuff: a case-based review. *Sports Med Arthrosc* 2017;25:164–71.
- [10] Cho NS, Cha SW, Rhee YG. Funnel tenotomy versus intracuff tenodesis for lesions of the long head of the biceps tendon associated with rotator cuff tears. *Am J Sports Med* 2014;42:1161–8.
- [11] Dosovitskiy A, Beyer L, Kolesnikov A, Weissenborn D, Zhai X, Unterthiner T, et al. An image is worth 16×16 words: transformers for image recognition at scale. *arXiv preprint arXiv:201011929*. 2020.
- [12] Kaplan E, Ekinci T, Kaplan S, Barua PD, Dogan S, Tuncer T, et al. PFP-LHCINCA: pyramidal fixed-size patch-based feature extraction and chi-square iterative neighborhood component analysis for automated fetal sex classification on ultrasound images. *Contrast Media Mol Imaging* 2022.
- [13] Baygin M, Yaman O, Barua PD, Dogan S, Tuncer T, Acharya UR. Exemplar darknet19 feature generation technique for automated kidney stone detection with coronal CT images. *Artif Intell Med* 2022;127:102274.
- [14] Baygin M, Dogan S, Tuncer T, Barua PD, Faust O, Arunkumar N, et al. Automated ASD detection using hybrid deep lightweight features extracted from EEG signals. *Comput Biol Med* 2021;134:104548.
- [15] Simonyan K, Zisserman A. Very deep convolutional networks for large-scale image recognition. *arXiv preprint arXiv:14091556*. 2014.
- [16] Tuncer T, Dogan S, Özuyurt F, Belhaouari SB, Bensmail H. Novel multi center and threshold ternary pattern based method for disease detection method using voice. *IEEE Access* 2020;8:84532–40.
- [17] Peterson LE. K-nearest neighbor. *Scholarpedia* 2009;4:1883.
- [18] Vapnik V. The support vector method of function estimation. *Nonlinear modeling*. Springer; 1998. p. 55–85.
- [19] Vapnik V. *The nature of statistical learning theory*. Springer science & business media; 2013.
- [20] Manzoor I, Kumar N. A feature reduced intrusion detection system using ANN classifier. *Expert Syst Appl* 2017;88:249–57.
- [21] Tolstikhin I., Houlsby N., Kolesnikov A., Beyer L., Zhai X., Unterthiner T., et al. MLP-Mixer: an all-MLP architecture for vision. *arXiv preprint arXiv:210501601*. 2021.
- [22] Chicco D, Jurman G. The advantages of the Matthews correlation coefficient (MCC) over F1 score and accuracy in binary classification evaluation. *BMC Genomics* 2020;21:6.
- [23] Warrens MJ. On the equivalence of Cohen's kappa and the Hubert-Arabie adjusted rand index. *J Classification* 2008;25:177–83.
- [24] Morag Y, Jacobson JA, Miller B, De Maeseneer M, Girish G, Jamadar D. MR imaging of rotator cuff injury: what the clinician needs to know. *Radiographics* 2006;26:1045–65.
- [25] Zhang X, Gu X, Zhao L. Comparative analysis of real-time dynamic ultrasound and magnetic resonance imaging in the diagnosis of rotator cuff tear injury. *Evid-Based Complement Altern Med* 2021:2021.
- [26] Krizhevsky A, Sutskever I, Hinton GE. Imagenet classification with deep convolutional neural networks. *Commun ACM* 2017;60:84–90.
- [27] Matcuk Jr GR, Moin P, Cen S. Shoulder measurements on MRI: statistical analysis of patients without and with rotator cuff tears and predictive modeling. *Clin Anatomy* 2020;33:173–86.
- [28] Jiang H, Chen L, Yj Zhao, Zy Lin, Yang H. Machine learning-based ultrasomics for predicting subacromial impingement syndrome stages. *J Ultrasound Med* 2021.
- [29] Kang Y, Choi D, Lee KJ, Oh JH, Kim BR, Ahn JM. Evaluating subscapularis tendon tears on axillary lateral radiographs using deep learning. *Eur Radiol* 2021;31:9408–17.